2022

Honey badger optimizer for extracting the ungiven parameters of PEMFC model: Steady-state assessment

Hossam Ashraf
The British University in Egypt, hossam.ashraf@bue.edu.eg

Sameh Osama Abdellatif Dr
The British University in Egypt, sameh.osama@bue.edu.eg

Mahmoud Elkoly dr
Zagazig University, melkholy71@yahoo.com

Attia Elfergany Prof
Zagazig University, el_fergany@ieee.org

Energy Conversion and Management 258 (2022) 115521

Contents lists available at ScienceDirect

Energy Conversion and Management

journal homepage: www.elsevier.com/locate/enconman

Honey badger optimizer for extracting the ungiven parameters of PEMFC model: Steady-state assessment

Hossam Ashraf [a], Sameh O. Abdellatif [a], Mahmoud M. Elkholy [b], Attia A. El-Fergany [b]

[a] Electrical Engineering Department, Faculty of Engineering and FabLab in the Centre for Emerging Learning Technologies (CELT), The British University in Egypt (BUE), Cairo, Egypt
[b] Electrical Power and Machines Department, Zagazig University, 44519 Zagazig, Egypt

ARTICLE INFO

Keywords:
Proton exchange membrane fuel cell
Mann's model
Parameter estimation
Honey badger optimizer
Sum of quadratic errors

ABSTRACT

In this work, a novel attempt is performed to optimally identify the seven ungiven parameters of the proton exchange membrane fuel cells (PEMFCs) steady-state model. A fitness function is adapted to reduce the sum of quadratic errors (SQEs) between the experimentally measured voltages and the corresponding computed values. A honey badger optimizer (HBO) is utilized to minimize the SQEs, exposed to a group of inequality bounds. Three test cases of well-known commercial PEMFCs units as benchmarking are elucidated and discussed over different steady-state operating conditions. Substantial comparisons to the other up-to-date optimizers published in the art-of-literature are provided to appraise the HBO's viability. It's worth highlighting that the values of maximum percentage biased voltage deviations for Ballard Mark, SR-12 and 250 W stacks are equal to 2.696%, −0.016% and 1.595%, respectively. Besides, several statistical measures are applied to indicate the proposed HBO robustness and accurateness. Furthermore, a sensitivity study based on SOBOL indicators is performed at which the influence of small deviations of the seven extracted parameters on the PEMFC's model, is comprehensively illustrated. It can be confirmed that the HBO asserts its capability to tackle this task effectively rather than others.

1. Introduction

At the present time, fuel cells (FCs) have been regarded as the new trend of the renewable-based energy conversion technology due to their robustness, higher efficiencies, and environmental friendship. Thus, FCs have penetrated the markets upon wide range of applications (stationary, portable, and transportation) for either residential, commercial, or industrial sectors. Based on the electrolyte material, FCs are classified into several types. Each type exhibits distinctive characteristics in terms of the operating temperatures, the power range, the electrical efficiencies, and the suitable applications [1,2]. Examples of such types are alkaline FCs [3], proton exchange membrane FCs [4], phosphoric acid FCs [5], solid oxide FCs [6], and many more.

Amongst the various FCs' types, proton exchange membrane FCs (PEMFCs) have impressively attracted the interests of the manufacturers and the customers as a result of their advantageous features. Despite PEMFCs' merits, their competitive spread into the commercial market suffers from their catalyst expensive cost [1,2,7]. Moreover, the PEMFC's output voltage is unregulated, caused by the operating losses, such that it decreases non-linearly with increasing the load. Particularly, the PEMFC's voltage starts with high decay due to the activation losses, then it diminishes linearly due to the ohmic losses, again it rapidly decreases at higher loads due to the concentration losses [8–10].

Consequently, the PEMFC modelling is a heavy nonlinear task which requires precise techniques to properly evaluate the PEMFC performance, and accurately simulate the electrical features of the PEMFC stacks [11]. Hence, several researchers have introduced many models to deal with the PEMFC operation aspects. Generally, the PEMFC models can be classified into; mechanistic [12], empirical [13], and semi-

Abbreviations: FCs, Fuel Cells; PEMFCs, Proton Exchange Membrane Fuel Cells; MHOs, Metaheuristic Optimizers; GO, Grasshopper Optimizer; GWO, Grey Wolf Optimizer; SSO, Shark Smell Optimizer; WO, Whale Optimizer; BO, Bonobo Optimizer; CHHO, Chaotic Harris Hawk Optimizer; CO, Coyote Optimizer; MRFO, Manta Rays Foraging Optimizer; BWO, Black Widow Optimizer; JSO, Jellyfish Search Optimizer; PFO, Pathfinder Optimizer; TSA, Tree-Seed Algorithm; STSA, Sine Tree-Seed Algorithm; GBO, Gradient-Based Optimizer; IAEO, Improved Artificial Ecosystem Optimizer; NNO, Neural Network Optimizer; SMO, Slime Mould Optimizer; TGO, Tree Growth Optimizer; MPO, Marine Predator Optimizer; PO, Political Optimizer; FPO, Flower Pollination Optimizer; HBO, Honey Badger Optimizer; OF, Objective Function; SQEs, Sum of Quadratic Errors; ICs, Inequality Constraints; TSO, Tona-Swarm Optimizer; ESMO, Equilibrium Slime Mould Optimizer; StD, Standard Deviation; GSS, Global Sensitivity Study.

E-mail addresses: Hossam.Ashraf@bue.edu.eg (H. Ashraf), el_fergany@zu.edu.eg (A.A. El-Fergany).

https://doi.org/10.1016/j.enconman.2022.115521
Received 8 December 2021; Received in revised form 18 February 2022; Accepted 17 March 2022

Nomenclatures

V_c	Output voltage of a single PEMFC (V)
E	Nernest open-circuit voltage (V)
V_{act}	Activation voltage decline (V)
V_Ω	Ohmic voltage drop (V)
V_{con}	Concentration voltage drop (V)
V_s	Output voltage of PEMFC stack (V)
N	Number of series PEMFCs
T_c	Cell operating temperature (K)
P_{H_2}, and P_{O_2}	Partial pressures of H_2 and O_2 (atm), respectively
I_c	Cell operating current in (A)
A_m	membrane effective area (cm^2)
R_{D_a}, and R_{D_c}	Relative dampness of the water vapor at the anode and cathode; respectively
P_a, and P_c	Inlet pressures of anode and cathode (atm)
P_{H_2O}	Saturation pressure of the water vapor (atm)
$\varepsilon_i(i = 1:4)$	Semi-empirical coefficients ($V, VK^{-1}, VK^{-1}, VK^{-1}$)
C_{O_2}	Concentration of O_2 at the catalytic layer (mol/cm^3)
R_m	Membrane resistance (Ω)
R_e	External connections resistance (Ω)
l	Membrane thickness (cm)
ρ_m	Membrane specific resistivity ($\Omega.cm$)
γ	Unitless parameter that indicates the dehydration status
β	Parametric factor (V)
J_M	Maximum current density (A/cm^2)
V_{meas}	Experimentally measured voltages
V_{calc}	Model-based calculated voltages
N_{pop}	Population size
$X(i)$	Position of the i^{th} honey badger in the related population
m, and $m_i(i = 1:7)$	Stochastic numbers from 0 to 1
ll_i, and hl_i	Lower and higher limits of the search space
$I(i)$	Smell intensity of the honey badger
C_p	Concentration of the prey
r_i	Distance between the i^{th} honey badger and the prey
$X(p)$	Prey position
ϑ	Density parameter
it, and it_{max}	Current iteration and maximum number of iterations
C	Constant ≥ 1
F	Flag
$X(new)$	Updated badgers' positions
σ	Foraging capability of the honey badger
f_i, and f_p	Fitness of the corresponding i^{th} agent and the prey best positions; respectively
$V_{\%BD}$	Percentage biased voltage deviation
S_i	1st order indicators
SO_i	Overall order indicators
K	number of measured dataset points

empirical models [14]. For more details about the various modeling categories, the reader can refer to [15–19].

Such models have their own mathematical formulations consisting of some unspecified parameters that aren't illustrated in the manufacturer's datasheets and need to be fully defined to construct a robust and effective model [20]. Therefore, numerous attempts have been carried out to properly identify the unknown parameters of the PEMFC models. Example of such attempts are electrochemical impedance spectroscopy-based techniques [21,22], black box-based approaches [23], adaptive filter-based [24] and current switching methods [25] and many more. Nevertheless, these techniques aren't widely adopted to obtain the unknown parameters of PEMFC as they aren't flexible and practicable [4].

Herein, a semi-empirical electrochemical model introduced by Mann et al [26], has been developed to simulate the electrical performance of PEMFC under steady state operation. Over the last two decades, Mann's model has attained wide approval for its capability of foreseeing the polarization characteristics of PEMFC under various operating conditions. However, in addition to the nonlinearity issue, the unknown parameters of Mann's model are strongly coupled and vary extremely with the load conditions. Accordingly, constructing the model using the aforesaid conventional methods has become more sophisticated and time-wasting [4].

Recently, due to the significant development of the artificial intelligent-based methods, a respected number of researchers have implemented the metaheuristic optimizers (MHOs) for extracting the undefined parameters of the PEMFC model. Referring to the PEMFC parameter estimation as an optimization problem, MHOs are the most reliable and effective tool to be applied [4,7,11].

Among such optimizers, that have been employed, are grasshopper optimizer (GO) [27], grey wolf optimizer (GWO) [28], shark smell optimizer (SSO) [29], whale optimizer (WO) [30] and bonobo optimizer (BO) [31]. Besides, chaotic Harris hawk optimizer (CHHO) [32], coyote optimizer (CO) [33], manta rays foraging optimizer (MRFO) [34], black widow optimizer (BWO) [35], jellyfish search optimizer (JSO) [36] and pathfinder optimizer (PFO) [37] have been applied for the same issue. Additively, the authors in [37–40] have utilized tree-seed algorithm (TSA) and sine tree-seed algorithm (STSA), gradient-based optimizer (GBO), improved artificial ecosystem optimizer (IAEO), and neural network optimizer (NNO), respectively, for the same purpose. At same context, the researchers have used slime mould optimizer (SMO) [41], tree-growth optimizer (TGO) [42], marine predator optimizer (MPO) and political optimizer (PO) [43], and flower pollination optimizer (FPO) [44] and many more [45–48].

It's clear from the above literature review that identifying the PEMFC unceratin parameters is a hot research point, where all the afore optimizers compete to get lower errors and lesser computational effort, smooth and fast convergence pattern, and better statistical indices. The above-mentioned competition is based on the no free-lunch theory that states there is no ultimate algorithm can solve all engineering optimization problems perfectly [45]. The aforesaid has motivated the authors to examine the performance of a novel swarm-based MHO, called honey badger optimizer (HBO) developed in 2022 [49] for pinpointing the uncertain parameters of three well-known PEMFCs stack test cases. It's noteworthy that the HBO has noticeable merits such as better transition between exploration and exploitation to evade getting trapped into local minima, fast convergence trend and lesser computational time. It's worth indicating that as far the authors' knowledge after an accurate search, this is the first application of HBO in the PEMFC's parameter estimation problem.

It's worth highlighting that the main contributions of this paper include: (i) executing and testing the performance of HBO to generate the optimal values of Mann's model unknowns, (ii) three typical test cases called Ballard Mark V, AVISTA SR-12, and 250 W stacks are deeply studied and (iii) various statistical comparisons to other recent competitive optimizers are done.

This article is structured as follows: Section 1 gives a brief literature review and the inspiration of the current effort. Section 2 discusses the mathematical formulation of well-matured Mann's model. The proposed objective function (OF) and the corresponding constraints are illustrated in Section 3. The procedures of HBO are indicated in Section 4. Section 5 reveals set of numerical simulations of the PEMFC model under various steady-state scenarios, beside performing various statistical tests to examine the HBO performance. Finally, the conclusion and the future insights are announced in Section 6.

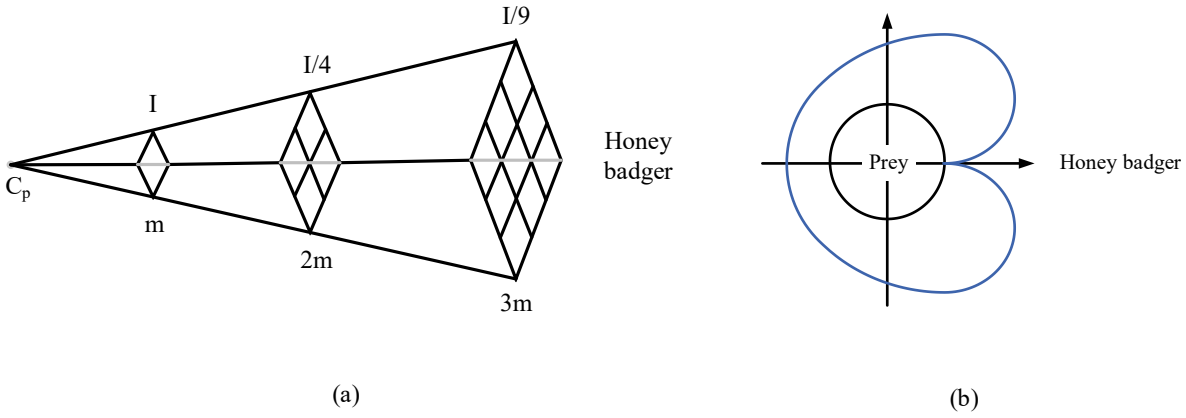

Fig. 1. Honey badger concepts: (a) Inverse square law and (b) The cardioid movement of the honey badger.

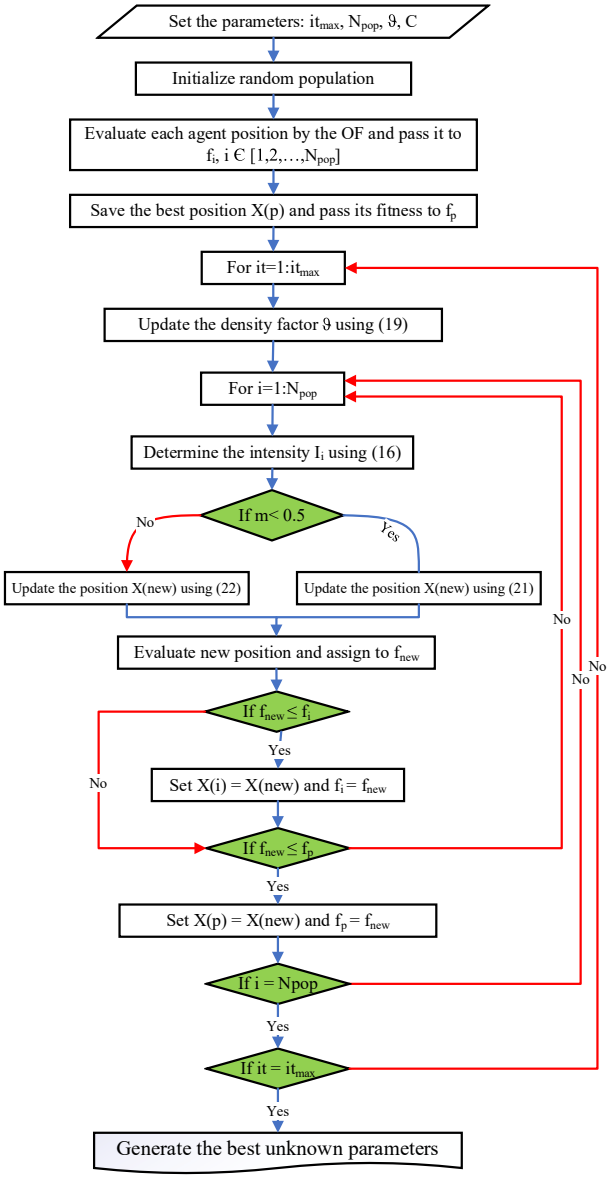

Fig. 2. The HBO flowchart.

2. Mathematical model of PEMFC

As earlier-stated, Mann's model has been considered as the most robust approach to represent the relation between the PEMFC output voltage and the drawn current in the steady state conditions. In addition, this model can also be extended further to transient conditions as well. The coming few statements briefly demonstrate this Mann's model as widely used in the literature. The overall output voltage of an individual PEMFC V_c in (V), can be expressed by (1) [26].

$$V_c = E - V_{act} - V_{\Omega} - V_{con} \tag{1}$$

Typically, the cell output voltage varies from 0.9 to 1.23 V based on the heating level and regulating pressures. So, to obtain higher voltage values, N cells have to be serially connected forming a PEMFCs stack V_s, as given by (2) [30,36].

$$V_s = N.V_c \tag{2}$$

However, equation (2) assumes that all cells act identically without any deviations.

Firstly, E can be determined by (3) for $T_c \leq 100^{\circ}\mathrm{C}$ [30–38].

$$E = 1.229 - 8.5 \times 10^{-4}(T_c - 298.15) + 4.3085 \times 10^{-5} \times T_c\left[ln\left(P_{H_2}\sqrt{P_{O_2}}\right)\right] \tag{3}$$

P_{H_2} and P_{O_2} are the partial pressures of H_2 and pure O_2 in (atm), which can be described by (4) and (5), respectively [36].

$$P_{H_2} = 0.5.R_{D_a}.P_{H_2O}.\left[\left[\frac{1}{\frac{R_{D_a}.P_{H_2O}}{P_a}.exp\left(\frac{1.635I_c}{A_m.T_c^{1.334}}\right)}\right] - 1\right] \tag{4}$$

$$P_{O_2} = R_{D_c}.P_{H_2O}.\left[\left[\frac{1}{\frac{R_{D_c}.P_{H_2O}}{P_c}.exp\left(\frac{4.192I_c}{A_m.T_c^{1.334}}\right)}\right] - 1\right] \tag{5}$$

P_{H_2O} symbolizes the saturation pressure of the water vapor in (atm), which can be given by (6) [27,36].

$$log_{10}(P_{H_2O}) = 2.95.10^{-2}(T_c - 273.15) - 9.18.10^{-5}(T_c - 273.15)^2 + 1.44.10^{-7}(T_c - 273.15)^3 - 2.18 \tag{6}$$

Secondly, V_{act} can be calculated by (7) [4,7].

$$V_{act} = -[\varepsilon_1 + \varepsilon_2.T_c + \varepsilon_3.T_c.ln(C_{O_2}) + \varepsilon_4.T_c.ln(I_c)] \tag{7}$$

where, $\varepsilon_i (i = 1:4)$ are semi-empirical coefficients in (V, VK^{-1}, VK^{-1},

Table 1
Datasheets of the study cases and the typical boundaries of the unknown parameters.

Stack type	Technical specifications			Practical boundaries		
	Mark V FC	SR-12	250 W	Parameter	minimum	maximum
N	35	48	24	$\varepsilon_1(V)$	−1.19997	−0.85320
$l(\mu m)$	178	25	127	$\varepsilon_2.10^{-3}(V/K)$	0.8	6.0
$A_m(cm^2)$	50.6	62.5	27.0	$\varepsilon_3.10^{-5}(V/K)$	3.6	9.8
$J_m(A/cm^2)$	1.500	0.672	0.860	$\varepsilon_4.10^{-5}(V/K)$	−26.00	−9.54
$T_c(K)$	343	323	343	γ	13	23
$P_{H_2}(atm)$	1.50000	1.47628	1.00000	$R_e(m\Omega)$	0.1	0.8
$P_{O_2}(atm)$	1.00000	0.20950	1.00000	$\beta(V)$	0.0136	0.5000

Table 2
HBO results compared to other challenging optimizers for Ballard Mark V.

Optimizer Parameters	**HBO**	TSO	ESMO	PFO [37]	STSA [37]	TSA [37]	GO [27]	NNO [40]	WO [30]
$\varepsilon_1(V)$	**−1.19970**	−0.85520	−0.85320	−1.19967	−0.85320	−1.19970	−0.85320	−0.97997	−1.19780
$\varepsilon_2.10^{-3}(V/K)$	**4.33453**	2.72227	2.54055	3.95786	2.55805	3.56765	3.41730	3.69460	4.41830
$\varepsilon_3.10^{-5}(V/K)$	**9.20688**	4.86143	3.60422	6.39011	3.60438	3.60000	9.80000	9.08710	9.72140
$\varepsilon_4.10^{-5}(V/K)$	**−16.28304**	−16.28305	−16.28244	−16.28300	−16.28280	−16.28300	−15.95550	−16.28200	−16.27300
γ	**23.00000**	23.00000	23.00000	23.00000	23.00000	23.00000	22.84580	23.00000	23.00000
$R_e(m\Omega)$	**0.10000**	0.10000	0.10000	0.10000	0.10000	0.10000	0.10000	0.10000	1.00200
$\beta(V)$	**0.01360**	0.01360	0.01360	0.01360	0.01360	0.01360	0.01360	0.01360	0.01360
$SQE(V^2)$	**0.853608**	0.853608	0.853608	0.853610	0.853610	0.853610	0.871000	0.853610	0.853700
it_{max}	**300**	300	300	200	3000	2000	100	100	200
N_{pop}	**30**	30	30	30	30	30	60	50	50

Table 3
HBO results compared to other challenging optimizers for AVISTA SR-12.

Optimizer Parameter	**HBO**	TSO	ESMO	SMO [29]	BWO [35]	BO [31]	TGO [42]	CHHO [32]	MPO [43]	FPO [44]
$\varepsilon_1(V)$	**−0.87299**	−0.85320	−1.17627	−0.97360	−1.09310	−1.09729	−1.11240	−0.85320	−1.02836	−1.05090
$\varepsilon_2.10^{-3}(V/K)$	**2.30398**	2.24255	4.12997	2.00000	1.20000	3.80925	3.85466	3.09184	3.89805	3.40000
$\varepsilon_3.10^{-5}(V/K)$	**3.60019**	3.60000	9.33731	9.47770	7.70000	9.80000	4.36986	8.23877	9.79999	6.58800
$\varepsilon_4.10^{-5}(V/K)$	**−10.6351**	−10.6370	−10.6364	−24.7220	−13.0000	−9.5400	−9.6448	−9.5400	−9.5400	−10.6220
γ	**21.09021**	13.00000	19.28074	17.33990	16.29970	23.00000	23.00000	22.91156	23.00000	12.79620*
$R_e(m\Omega)$	**0.26702**	0.10000	0.23983	0.30000	0.01440	0.67231	0.21887	0.62468	0.67231	0.19101
$\beta(V)$	**0.14998**	0.14864	0.149853	0.32150	0.50380*	0.17532	0.18307	0.17624	0.17532	0.22560
$SQE(V^2)$	**0.000142**	0.000310	0.000144	0.29595	0.03840	1.05663	1.104085	1.05716	1.05663	0.001881
it_{max}	**300**	300	300	1000	1000	200	500	500	3000	500
N_{pop}	**30**	30	30	NM	50	30	20	30	NM	NM

*The reported γ violates the stated limits (See Table 1). So, unfeasible solution. "NM" refers to "not mentioned".

Table 4
HBO results compared to other challenging optimizers for 250 W stack.

Optimizer Parameter	**HBO**	TSO	ESMO	JSO [36]	GBO [38]	IAEO [39]	BO [31]	CHHO [32]	CO [33]
$\varepsilon_1(V)$	**−0.85320**	−0.85391	−0.97123	−0.96089	−1.16647	−0.99910	−1.19969	−0.91010	−1.18542
$\varepsilon_2.10^{-3}(V/K)$	**2.25892**	2.25410	2.81252	3.21947	3.22560	2.82500	3.01886	2.96614	3.00508
$\varepsilon_3.10^{-5}(V/K)$	**3.60777**	3.60000	5.10588	8.11000	3.80178	4.47000	3.60000	7.78813	9.80000
$\varepsilon_4.10^{-5}(V/K)$	**−17.38902**	−16.11273	−17.37440	−17.48900	−17.48890	−17.00000	−15.5870	−15.23891	−12.06106
γ	**14.43913**	13.00000	14.411522	19.93580	19.03580	19.93580	23.00000	22.23630	23.00000
$R_e(m\Omega)$	**0.10000**	0.10000	0.10000	0.10000	0.10000	0.10000	0.10000	0.19321	0.10000
$\beta(V)$	**0.01379**	0.01360	0.01376	0.01453	0.01453	0.01450	0.05455	0.05367	0.06256
$SQE(V^2)$	**0.331371**	0.394386	0.331376	0.335980	0.335980	0.336000	0.642013	0.674730	0.613910
it_{max}	**300**	300	300	300	500	3000	200	500	1000
N_{pop}	**30**	30	30	30	50	50	30	30	100

VK^{-1}). C_{O_2} represents the O_2 concentration at the catalytic layer in (mol/cm^3), which can be referred in (8) [27,36].

$$C_{O_2} = \frac{P_{O_2}}{5.08.10^6}.exp(\frac{498}{T_c}) \tag{8}$$

Thirdly, V_Ω can be obtained from (9) [29–33].

$$V_\Omega = I_c(R_m + R_e); R_m = \rho_m\left(\frac{l}{A_m}\right) \tag{9}$$

ρ_m points out the membrane specific resistivity in ($\Omega.cm$), expressed in (10) [34–38].

$$\rho_M = \frac{181.6\left[1 + 0.03\left(\frac{I_c}{A_m}\right) + 0.062\left(\frac{T_c}{303}\right)^2\left(\frac{I_c}{A_m}\right)^{2.5}\right]}{\left[\gamma - 0.634 - 3\left(\frac{I_c}{A_m}\right)\right].exp\left(4.18\left(\frac{T_c-303}{T_c}\right)\right)} \tag{10}$$

It's worth emphasizing that γ represents the membrane water content and its assessment is a challenging matter due to its variation during the cell operation. In this work, it may be asserted that a convenient water content, at all probable operating scenarios, is assumed constant.

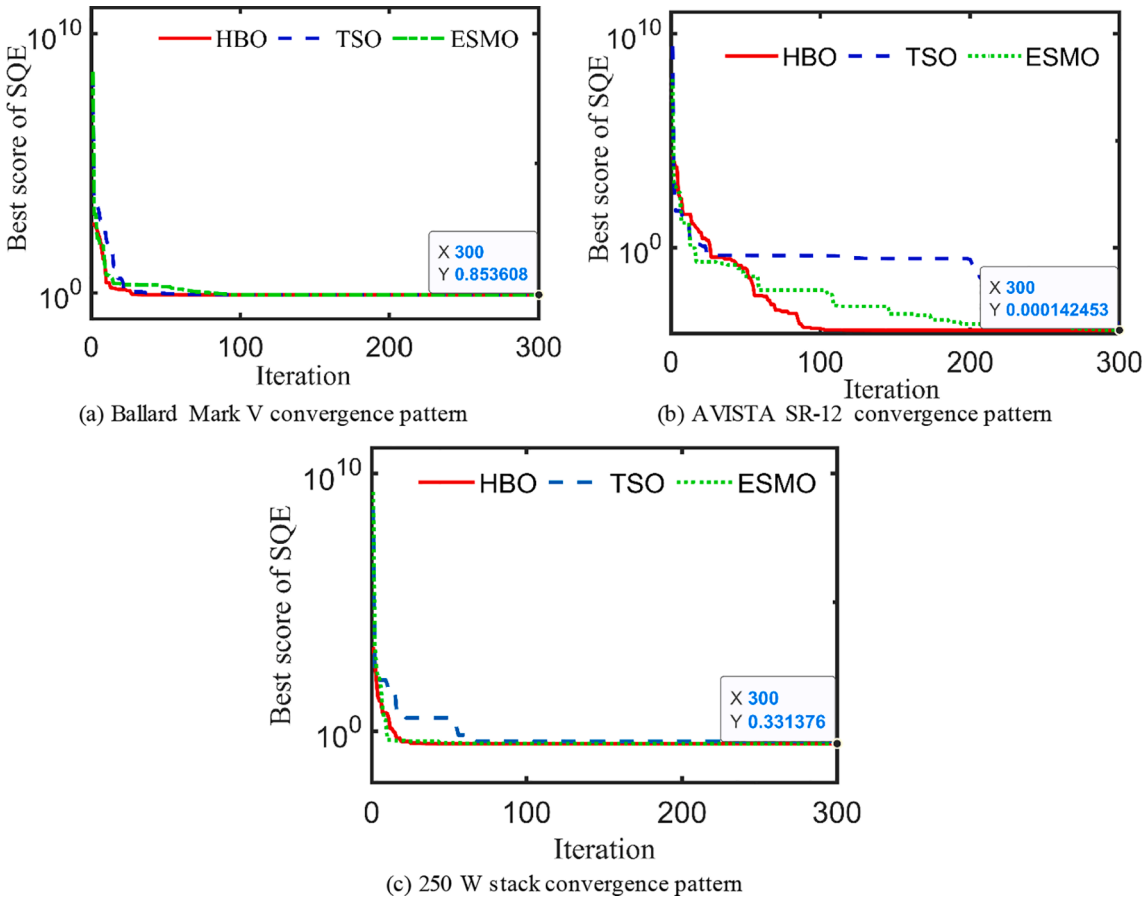

(a) Ballard Mark V convergence pattern

(b) AVISTA SR-12 convergence pattern

(c) 250 W stack convergence pattern

Fig. 3. Trend of SQE convergences for the study cases.

Finally, V_{con} can be appraised by (11) [29–38].

$$V_{con} = -\beta ln\left(1 - \frac{I_c}{A_m . J_M}\right) \tag{11}$$

According to the above-mentioned equations, it's obvious that there are seven undefined parameters ($\varepsilon_1, \varepsilon_2, \varepsilon_3, \varepsilon_4, \gamma, R_e and \beta$) which are not existed in the fabricators' datasheets. These parameters will be optimized using the proposed HBO to attain a precise PEMFC steady-state modelling under different operating circumstances.

3. Problem formulation

For the sake of estimating the seven ungiven variables of PEMFC, the sum of quadratic errors (SQEs) between the experimentally recorded voltages V_{meas} and the computed voltages V_{calc} using the afore model is employed. The SQE that is described in (12), is broadly utilized in the literatures [10,27,29–38,46–48]. Seeking for fair comparison to the other published optimizers, the OF is adopted to minimize the SQE, as revealed in (13).

$$SQE = \sum_{j=1}^{K} \left(V_{meas,j} - V_{calc,j}\right)^2 \tag{12}$$

$$OF = Minimize(SQE) \tag{13}$$

Moreover, the SQE is subjected to set of inequality constraints (ICs), as indicated in (14).

$$ICs = \begin{cases} \varepsilon_{n,min} \le \varepsilon_n \le \varepsilon_{n,max} \forall n \in 1:4 \\ \gamma_{,min} \le \gamma_n \le \gamma_{max} \\ R_{e,min} \le R_e \le R_{e,max} \\ \beta_{min} \le \beta \le \beta_{max} \end{cases} \tag{14}$$

It's known that the searching through the lower and higher limits of the previous ICs are preserved by HBO (self-constrained without any additional burdens to the OF). The ultimate target is to attain significant fitting between the experimental/recorded output voltages and the corresponding estimated ones by the HBO-based outcomes.

4. Procedures of the HBO

HBO is a swarm-based MHO introduced by Hashim et al. [49]. Principally, HBO is inspired by the intelligent attitudes of honey badger when searching for food (bee honey). For targeting the prey places, the honey badger utilizes one of two techniques. The first one is to depend on its smell sense to approximately locate the food source then start digging to catch the prey. While the other one is to follow the honey-guide bird guides to directly detect the beehive. Regarding more details about the inspiration and motivation of HBO, the reader is invited to browse [49–51].

Specifically, HBO is divided into two stages; the digging stage and the honey stage which represent the exploration and exploitation phases of the proposed optimizer. To mathematically formulate HBO, the first step is to initialize the population size N_{pop} which refers to the honey badgers with their corresponding positions, as indicated in (15).

$$X(i) = ll_i + m_1 \times (hl_i - ll_i) \tag{15}$$

The second step is to define the smell intensity of the honey badger $I(i)$

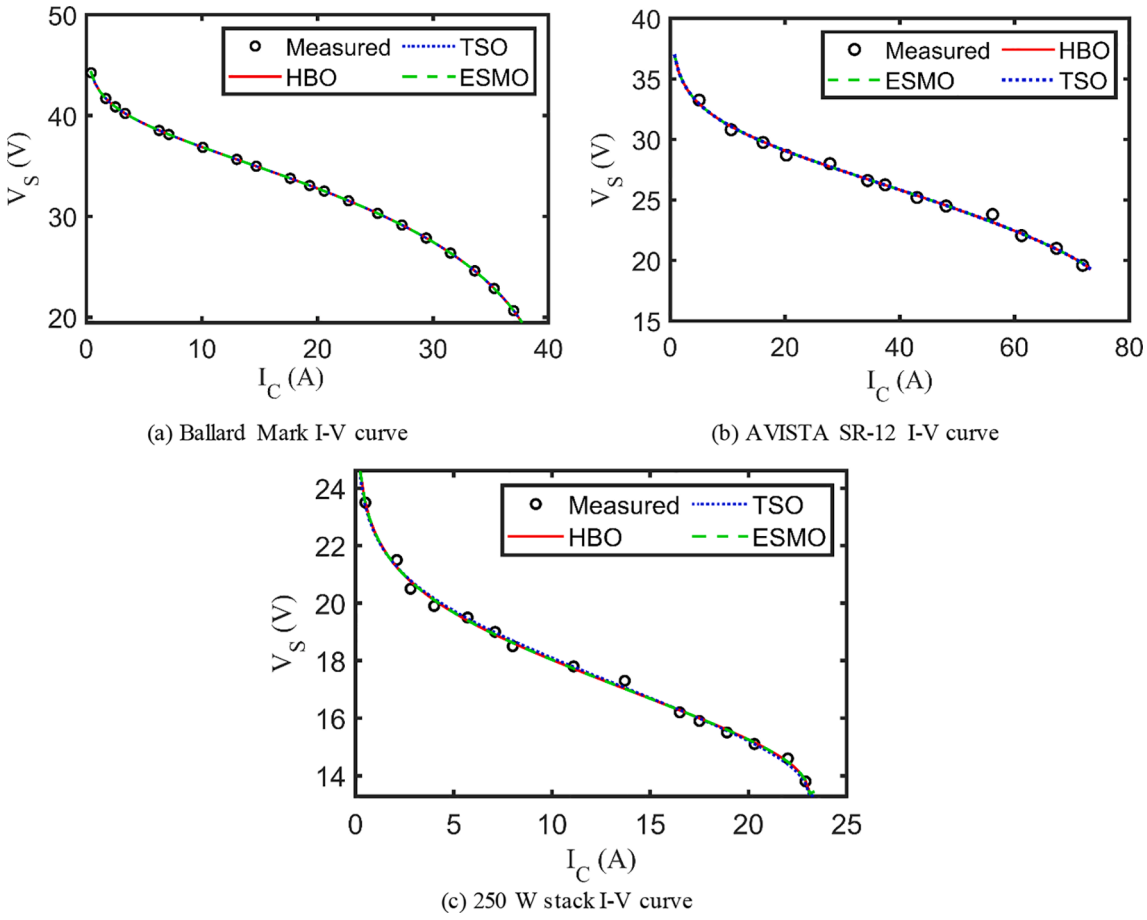

(a) Ballard Mark I-V curve

(b) AVISTA SR-12 I-V curve

(c) 250 W stack I-V curve

Fig. 4. Plots of I-V curves.

towards the prey. According to Inverse Square Law, the intensity is a function of the prey concentration and the distance between the prey and the honey badger. Consequently, the higher $I(i)$ is, the faster movement will be and vice versa, as depicted in (16)-(18) and revealed in Fig. 1(a).

$$I(i) = m_2 \times \frac{C_p}{4\pi r_i^2} \tag{16}$$

$$C_p = (X(i) - X(i+1))^2 \tag{17}$$

$$r_i = (X(p) - X(i)) \tag{18}$$

The third step is to update the density parameter ϑ which controls the haphazardness rate to guarantee smooth transformation from exploration to exploitation phases. Furthermore, ϑ updates its value relying on the current iteration it and the maximum number of iterations it_{max}, as given in (19).

$$\vartheta = C \times e^{\left(\frac{-it}{it_{max}}\right)} \tag{19}$$

To avoid getting stuck into local optima, the suggested optimizer employs a flag F which changes the search direction for obtaining high chances for agents to accurately cover the search area. F is mathematically formulated by (20).

$$F = \begin{cases} -1, if m_3 \le 0.5 \\ 1, else \end{cases} \tag{20}$$

Eventually, it's time to update the badgers' positions $X(new)$. As earlier-mentioned, the update process is achieved through the digging and honey activities. Particularly, in the digging stage, the agent motion imitates a heart shape, as shown in Fig. 1(b) and described by (21).

$$X(new) = X(p) + F \times \sigma \times I \times X(p) + F \times m_4 \times \vartheta \times r_i |\cos(2\pi m_5) \times [1 - \cos(2\pi m_6)]| \tag{21}$$

Generally, during the digging activity, the agent position extremely depends on I, r and ϑ. However, the badger may receive any flag F which guides it to explore even better food sources.

On the other hand, the honey phase is implemented when the badger follows the bird to locate a beehive which can be simulated by (22).

$$X(new) = X(p) + F \times m_7 \times \vartheta \times r_i \tag{22}$$

Mainly, during the honey activity, the badger exploits the bird guides to implement a search near to the prey position discovered by the bird. Besides, the search process is affected by density factor ϑ, while the badger may be notified by a flag F. It's self-explanatory that only C, σ, N_{pop} and it_{max} have to be set by the user leading to lesser computational effort and random trials to fine-control the performance of HBO. The reader can easily track the general steps of the proposed HBO in the flowchart revealed in Fig. 2.

5. Study cases, simulations, and optimizer validations

Herein, three commercial PEMFCs, widely utilized in the literatures, are employed to prove the robustness and effectiveness of the supposed HBO-based methodology under steady-state operation. For ensuring unprejudiced comparisons to other competitive optimizers, the parameters' boundaries, commonly mentioned in the state-of-art, have been unified for all study cases. It's worth saying that the numerical simulations are executed via MATLAB version R2018b on a laptop device with

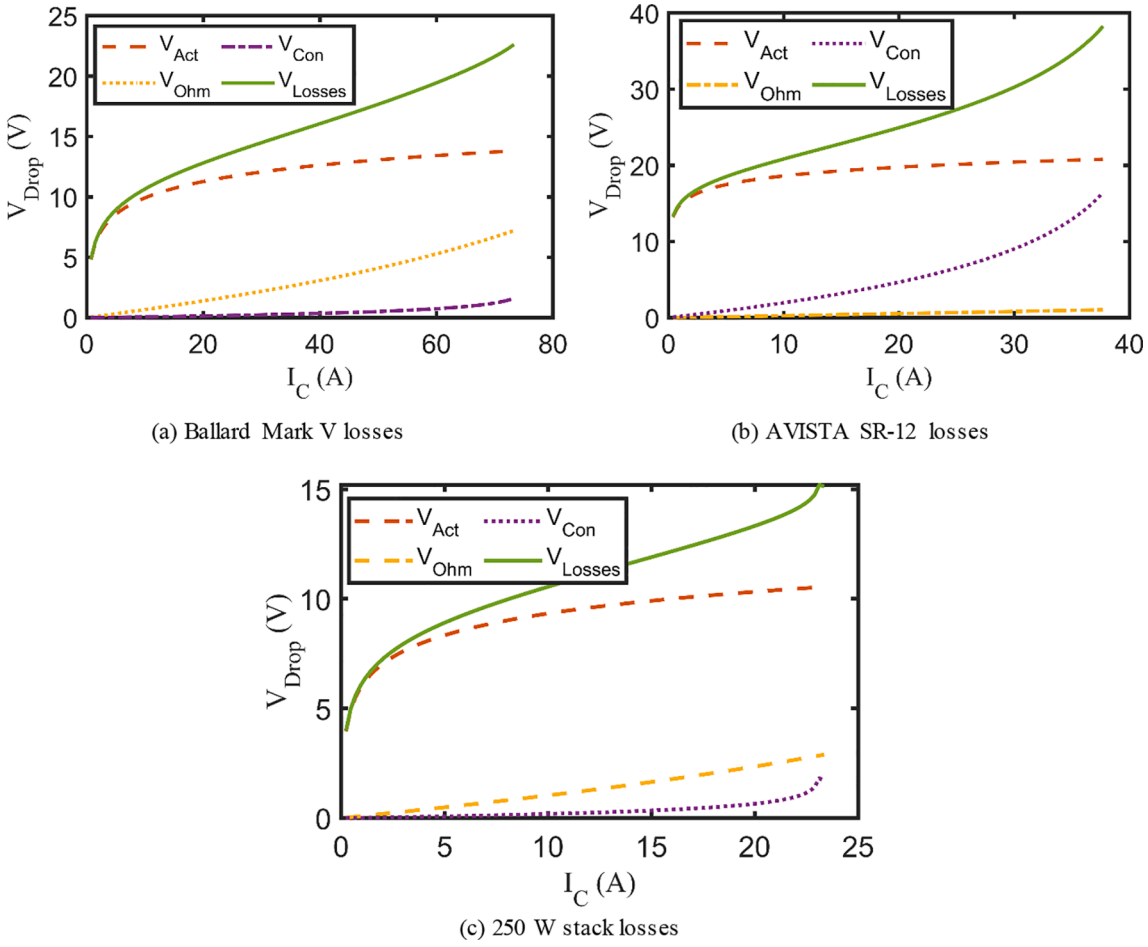

(a) Ballard Mark V losses

(b) AVISTA SR-12 losses

(c) 250 W stack losses

Fig. 5. Plots of the activation, ohmic and concentration losses, total losses, and Nernst voltage.

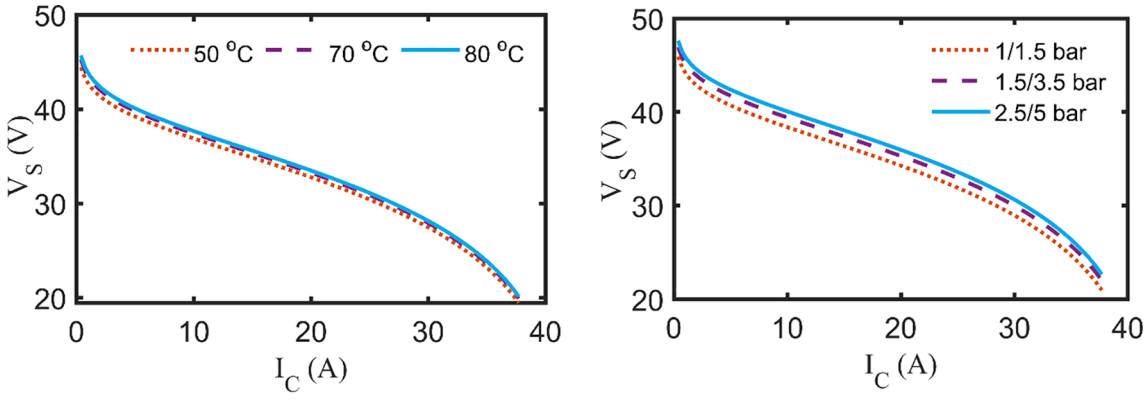

(a) I-V curves at changeable temperatures

(b) I-V curves at changeable supply pressures

Fig. 6. Polarization curves of AVISTA SR-12 under various operating conditions.

Intel Core i7 CPU, and 8 GB RAM (OS: Windows 10 Enterprise).

Furthermore, the values of the HBO tunning parameters are $N_{pop} = 30$, $it_{max} = 300$, $C = 6$ and $\sigma = 2$. Besides, the optimized values of the unidentified parameters are captured after running HBO 50 independent executions because of the high haphazardness concept of such approaches. Also, set of statistical tests are implemented to affirm the viability and the precision of the proposed HBO-methodology.

5.1. Study cases' technical specifications and the unknown parameters' limits

For uncomplicated referencing, the fabricators' datasheets of the previously-stated study cases are obtained from [27,28,36,37,38,42–44], which are shown in Table 1. In all cases, the relative dampness of water vapor at anode and cathode (R_{D_a} and R_{D_c}) are kept equal to 1.00. The lower and upper limits of the unknown parameters are gathered from [27,34,36,37,39,40,43,52], and revealed in Table 1 (last three columns).

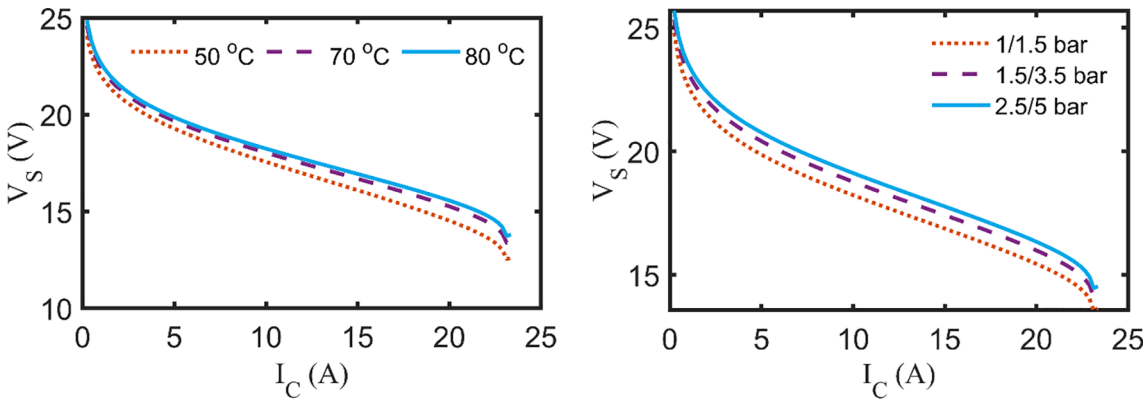

(a) I-V curves at changeable temperatures (b) I-V curves at changeable supply pressures

Fig. 7. Polarization curves of 250 W stack under various operating conditions.

Table 5
Statistical metrics of HBO and others.

Type	Optimizer	Parameters				Elapsed Time (s)
		Best	Mean	Worst	StD.10^{-3}	
Ballard Mark V	HBO	0.853608	0.989870	1.542909	274.83600	15.69
	TSO	0.853608	1.747287	2.281877	301.18200	14.55
	ESMO	0.853608	0.861271	0.982512	22.68297	16.37
AVISTA SR-12	HBO	0.000142	0.004465	0.036763	9.54149	22.81
	TSO	0.000310	0.098664	0.314069	50.92980	21.88
	ESMO	0.000144	0.012106	0.052198	12.71980	23.27
250 W Stack	HBO	0.331371	0.332919	0.345910	2.87497	16.79
	TSO	0.394386	1.316534	3.273921	964.59800	16.59
	ESMO	0.331376	0.333445	0.341634	2.54025	17.93

5.2. Parameters' estimations of the PEMFC study cases

In this subsection, HBO along with two new algorithms, called TSO [53] and ESMO [54], are applied to optimally generate the unknown parameters of the PEMFC model. The results of lowest SQE values of total 50 independent executions for Ballard Mark V, SR-12 and 250 W stacks, compared to the other two implemented optimizers and the recently-published works, are summarized in Tables 2–4, respectively. Moreover, the reader can browse the aforementioned Tables for the values of the optimized parameters, beside the iterations and populations numbers of each optimizer. The convergence patterns for the three cases under study via the executed optimizers are illustrated in Fig. 3(a)–(c).

It can be observed that HBO have superior convergence features rather than TSO and ESMO in terms of fast, smooth, and steady progress to the final optimal SQE value during 300 iterations. Fig. 4(a)–(c) illustrate the I-V curves of the experimental datasets along with the computed ones using the suggested HBO-based model, beside TSO and EMSO, for Mark V FC, SR-12 and 250 W stacks, respectively. Referring to Fig. 4(a)–(c), it may be noted that the simulated I-V curves, which are the output of the model after receiving the optimized values of the parameters, are compatible and well matching to the corresponding measured values. What's more, the insignificant SQE values assert the above-stated well agreeing claim (See Tables 2–4).

As formerly-stated, the polarization characteristics are affected by three losses: activation, ohmic, and concentration, where their dominance varies during the loading conditions [27,38]. In order to fully grasp such variations, Fig. 5(a)–(c) depict the variations of the previously-indicated losses with the load current along with the open-circuit voltage for Mark V, SR-12 and 250 W stacks, respectively. Closer look to Fig. 5(a)–(c), it may be obvious that the activation losses are dominant at startup, then a linear relationship is exhibited due to the ohmic losses, lastly, the activation losses dominate at higher loads.

5.3. Simulations under diverse steady-state circumstances

At this part, various operating conditions are submitted to evaluate the steady-state performance of PEMFC. Particularly, this section discusses the impact of varying the operating temperature T_c and the fuel and oxidant pressures P_{H_2}/P_{O_2} on the polarization characteristics of the PEMFC stacks. To avert lengthy paper, two of the three study cases are demonstrated for the above-stated aim. Specifically, after obtaining the optimum values of the unknown parameters by HBO (See Tables 2–4), the I-V curves of the SR-12 modular and the 250 W stack are generated under varying T_c with constant P_{H_2}/P_{O_2} and vice versa. The I-V curves of the SR-12 and the 250 W stacks at 50, 70 and 80 °C, respectively, under constant P_{H_2}/P_{O_2}, as mentioned in their datasheets, are depicted in Fig. 6 (a) and Fig. 7(a), respectively. Additionally, the polarization curves of the above-mentioned study cases at (1/1.5 bar), (1.5/3.5 bar) and (2.5/5 bar), respectively, under constant T_c, as stated in their technical specifications, are pursued in Fig. 6(b) and Fig. 7(b), respectively.

According to Fig. 6(a) and Fig. 7(a), the reader can clearly notice that the polarization features are enhanced by increasing the operating temperature T_c at constant supply pressures P_{H_2}/P_{O_2}. Furthermore, regarding Fig. 6(b) and Fig. 7(b), it can be realized that the output voltage can be improved by raising the supply pressures P_{H_2}/P_{O_2} at constant cell temperature T_c.

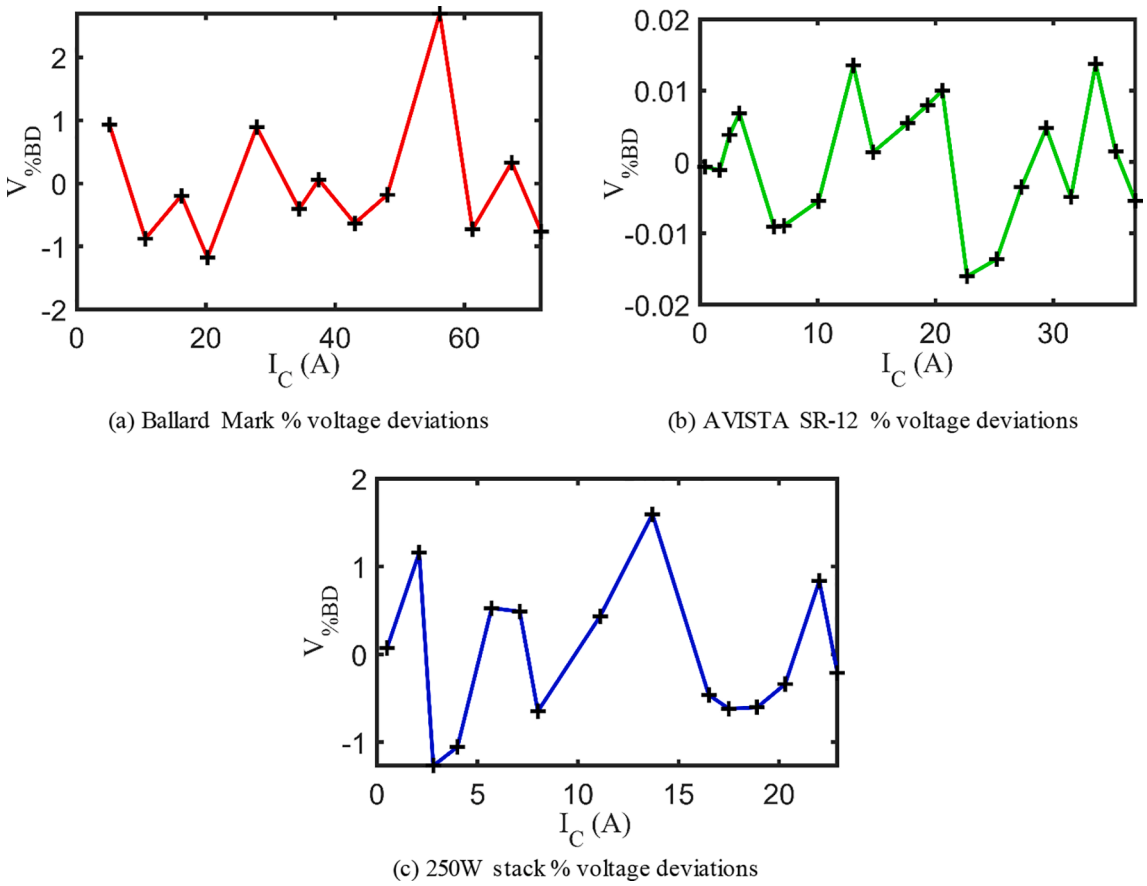

(a) Ballard Mark % voltage deviations

(b) AVISTA SR-12 % voltage deviations

(c) 250W stack % voltage deviations

Fig. 8. Plots of percentage voltage deviations.

Table 6
Sobol sensitivity indicators for the PEMFC extracted parameters.

Parameter	Ballard Mark FC		AVISTA SR-12		250 W stack	
	S_i	SO_i	S_i	SO_i	S_i	SO_i
ε_1	0.04388	0.70601	0.17086	0.88146	0.17299	0.84357
ε_2	0.17836	0.86899	0.07811	0.74525	0.09521	0.77351
ε_3	−0.01383	0.14653	0.00848	0.06912	0.02216	0.05935
ε_4	−0.01388	0.02386	0.01695	0.01592	−0.00504	0.03111
γ	−0.01424	0.00768	0.00645	6.27690×10^{-5}	0.00636	0.00863
R_e	−0.01577	1.02300×10^{-5}	0.00719	5.91620×10^{-5}	0.00705	2.57640×10^{-6}
β	−0.01565	1.21270×10^{-4}	0.01331	0.02495	0.00763	4.89870×10^{-4}

5.4. Statistical, sensitivity and performance validations

To appraise the robustness, effectiveness, and accurateness of HBO, set of parametric statistical metrics are performed such as the best, the mean, the worst, and the standard deviation (StD) of the adopted SQE after 50 independent runs. These statistical indices of HBO along with the executed optimizers for the three PEMFCs' study cases are encapsulated in Table 5. As known, the task of PEMFC parameters' identification is off-line process which means that reporting the simulation time is insignificant. Nevertheless, the elapsed time is stated in Table 5 (The last column).

Correspondingly, the percentage biased voltage deviation $V_{\%BD}$ has been employed to signify the reliability and precision of HBO in fitting the calculated output voltages with the measured ones. The variation of $V_{\%BD}$, which can be formulated by (23) [36], along with the corresponding load current values for the three earlier-stated study cases are depicted in Fig. 8(a)–(c), respectively. It may be useful mentioning that the maximum values of $V_{\%BD}$ for Ballard Mark, SR-12 and 250 W stacks are 2.696%, −0.016% and 1.595%, respectively.

$$V_{\%BD} = \frac{V_{meas} - V_{calc}}{V_{meas}} \times 100 \tag{23}$$

Over and above that, the global sensitivity study (GSS) is carried out to investigate the effect of changing the values of the PEMFC optimized parameters on the calculated SQE. Mainly, GSS is an effectual technique for estimating the variation impacts of certain parameters on their model performance. Actually, GSS is a function of Sobol sensitivity indicators S_i (1st order indicators) and SO_i (overall order indicators) which are determined by Monte Carlo simulations and imitated using easyGSS toolbox [55–57]. Particularly, S_i denote the effect of varying every single parameter on SQE, while SO_i show the overall effect of that parameter considering its interactive relations with the other parameters. Thus, the divergence between S_i and SO_i elucidates how strong the interactions among the model parameters are. Accordingly, in case of no interactions among the model parameters, S_i and SO_i are identical. Moreover, the higher S_i is, the more vital the parameter is [55,56]. In

this study, the variation range is picked as ±10% of the optimized values of the PEMFC parameters and the number of samples employed by Sobol GSS is 5×10^3. Table 6 summarizes the values of Sobol sensitivity indicators when changing each optimized parameter for the three study cases.

Generally, the reader can conclude that the PEMFC output voltage significantly depends on three parameters, called ε_1, ε_2 and ε_3 due to the corresponding high S_i and SO_i. On the contrary side, the output voltage sensitivity is moderate for ε_4 and γ, while modest sensitivity appears for R_e and β. Consequently, as formerly-demonstrated, the PEMFC model is a heavy nonlinear one, where any small variations of the extracted optimal parameters affect the model performance and especially for the afore-stated three parameters. The aforementioned appraises the HBO-based technique in generating the best values of the undefined parameters.

In addition to that, computational time complexity of the employed HBO is performed. In which, the HBO principally includes some stages as indicated in Fig. 2: initialization, evaluation of fitness, exploration and exploitation phases. In the considered formulas, N_{pop} denotes the population size, Dim defines the dimension of the problem/decision variables, and it_{max} is the total number of iterations. In this context, the computational complexity can be summarized as follows: The problem definition enforces $O(1)$ time, the initialization stage needs $O(N_{pop})$ time, the evaluation of fitness step needs $O(N_{pop})$ time, the updating process requires $O(it_{max})$ time, and the updating of locations of badgers' require $O(it_{max} \times Dim)$ time. Hence, the whole time complexity of HBO acquires Big-O as illustrated before. By omitting the constants and coefficients the final concluded Big-O of the HBO is specified in (24).

$$O(\text{HBO}) = O\left(N_{pop}.it_{max}.Dim\right) \tag{24}$$

6. Conclusions

An efficient tool based on HBO has been presented for extracting the ungiven parameters of the well-known PEMFC's model, namely Mann's model. Three test typical cases have been thoroughly demonstrated via numerical simulations in terms of the computed polarization characteristics and the losses' variations with the varied load current. Additionally, different steady-state conditions have been demonstrated and discussed under varied operating scenarios. The final best values of SQEs for Ballard Mark V FC, AVISTA SR-12 and 250 W stacks are 0.853608, 0.000142 and 0.331371 V^2, respectively. Statistically, HBO has exhibited a soft, fast, and stable convergence trend as evidenced by the patterns of plots. Moreover, the HBO has been tested under various statistical parametric indices to signify its robustness and effectiveness. Lastly, a sensitivity study based on SOBOL indicators has been implemented to see how dependent is the PEMFC's model on the optimized parameters. In addition to that, the computational complexity of the HBO has been carried out. Our future target is to test the performance of HBO in evaluating the transient/dynamic operation of various PEMFC stacks considering the impact of varying the suppliants' flow rates on the polarization features.

CRediT authorship contribution statement

Hossam Ashraf: Conceptualization, Methodology, Investigation, Software, Writing – original draft. **Sameh O. Abdellatif:** Data curation, Validation, Software, Writing – original draft. **Mahmoud M. Elkholy:** Data curation, Visualization, Software, Investigation, Writing – review & editing, Formal analysis. **Attia A. El-Fergany:** Software, Methodology, Writing – review & editing, Supervision, Validation.

Declaration of Competing Interest

The authors declare that they have no known competing financial interests or personal relationships that could have appeared to influence the work reported in this paper.

References

[1] Sharaf OZ, Orhan MF. An overview of fuel cell technology: fundamentals and applications. Renew Sustain Energy Rev 2014;32:810–53. https://doi.org/10.1016/j.rser.2014.01.012.

[2] Karanfil G. Importance and applications of DOE/optimization methods in PEM fuel cells: a review. Int J Energy Res 2020;44:4–25. https://doi.org/10.1002/er.4815.

[3] Saebea D, Chaiburi C, Authayanun S. Model based evaluation of alkaline anion exchange membrane fuel cells with water management. Chem Eng J 2019;374:721–9. https://doi.org/10.1016/j.cej.2019.05.200.

[4] Yang B, Wang J, Lei Y, Shu H, Tao Y, Zhang X, et al. A critical survey on proton exchange membrane fuel cell parameter estimation using meta-heuristic algorithms. J Cleaner Prod 2020;265:121660. https://doi.org/10.1016/j.jclepro.2020.121660.

[5] Inci M, Türksoy O. Review of fuel cells to grid interface: configurations, technical challenges and trends. J Cleaner Prod 2019;213:1353–70. https://doi.org/10.1016/j.jclepro.2018.12.281.

[6] Oryshchyn D, Harun NF, Tucker D, Bryden KM, Shadle L. Fuel utilization effects on system efficiency in solid oxide fuel cell gas turbine hybrid systems. Appl Energy 2018;228:1953–65.

[7] Ohenoja M, Leiviska K. Observations on the parameter estimation problem of polymer electrolyte membrane fuel cell polarization curves. Fuel Cells 2020;20:516–26. https://doi.org/10.1002/fuce.201900155.

[8] El-Hay EA, El-Hameed MA, El-Fergany AA. Improved performance of PEM fuel cells stack feeding switched reluctance motor using multi-objective dragonfly optimizer. Neural Comput Appl 2019;31:6909–24. https://doi.org/10.1007/s00521-018-3524-z.

[9] El-Hay EA, El-Hameed MA, El-Fergany AA. Performance enhancement of autonomous system comprising proton exchange membrane fuel cells and switched reluctance motor. Energy 2018;163:699–711. https://doi.org/10.1016/j.energy.2018.08.104.

[10] Shaheen MAM, Hasanien HM, El Moursi MS, El-Fergany AA. Precise modeling of PEM fuel cell using improved chaotic MayFly optimization algorithm. Int J Energy Res 2021:1–16. https://doi.org/10.1002/er.6987.

[11] Priya K, Sathishkumar K, Rajasekar N. A comprehensive review on parameter estimation techniques for Proton Exchange Membrane fuel cell modelling. Renew Sustain Energy Rev 2018;93:121–44. https://doi.org/10.1016/j.rser.2018.05.017.

[12] Giner-Sanz JJ, Ortega EM, Pérez-Herranz V. Mechanistic equivalent circuit modelling of a commercial polymer electrolyte membrane fuel cell. J Power Sources 2018;379:328–37. https://doi.org/10.1016/j.jpowsour.2018.01.066.

[13] Busquet S, Hubert CE, Labbé J, Mayer D, Metkemeijer R. A new approach to empirical electrical modelling of a fuel cell, an electrolyser or a regenerative fuel cell. J Power Sources 2004;134:41–8. https://doi.org/10.1016/j.jpowsour.2004.02.018.

[14] Han J, Han J, Ji H, Yu S. "Model-based" design of thermal management system of a fuel cell "air-independent" propulsion system for underwater shipboard. Int J Hydrogen Energy 2020;45(56):32449–63.

[15] Zhang G, Jiao K. Three-dimensional multi-phase simulation of PEMFC at high current density utilizing Eulerian-Eulerian model and two-fluid model. Energy Convers Manage 2018;176:409–21. https://doi.org/10.1016/j.enconman.2018.09.031.

[16] Peng F, Ren L, Zhao Y, Li L. Hybrid dynamic modeling-based membrane hydration analysis for the commercial high-power integrated PEMFC systems considering water transport equivalent. Energy Convers Manage 2020;205:112385. https://doi.org/10.1016/j.enconman.2019.112385.

[17] Liu G, Qin Y, Wang J, Liu C, Yin Y, Zhao J, et al. Thermodynamic modeling and analysis of a novel PEMFC-ORC combined power system. Energy Convers Manage 2020;217:112998.

[18] Chen Xi, Liu Q, Jianghai Xu, Chen Y, Li W, Yuan Z, et al. Thermodynamic study of a hybrid PEMFC-solar energy multi-generation system combined with SOEC and dual Rankine cycle. Energy Convers Manage 2020;226:113512. https://doi.org/10.1016/j.enconman.2020.113512.

[19] Xu Y, Fan R, Chang G, Xu S, Cai T. Investigating temperature-driven water transport in cathode gas diffusion media of PEMFC with a non-isothermal, two-phase model. Energy Convers Manage 2021;248:114791.

[20] Secanell M, Wishart J, Dobson P. Computational design and optimization of fuel cells and fuel cell systems: a review. J Power Sources 2011;196:3690–704. https://doi.org/10.1016/j.jpowsour.2010.12.011.

[21] Niya SMR, Hoorfar M. Study of proton exchange membrane fuel cells using electrochemical impedance spectroscopy technique e A review. J Power Sources 2013;240:281–93. https://doi.org/10.1016/j.jpowsour.2013.04.011.

[22] Taleb MA, Bethoux O, Godoy E. Identification of a PEMFC fractional order model. Int J Hydrogen Energy 2017;42:1499–509. https://doi.org/10.1016/j.ijhydene.2016.07.056.

[23] Kheirandish A, Motlagh F, Shafiabady N, Dahari M. Dynamic modelling of PEM fuel cell of power electric bicycle system. Int J Hydrogen Energy 2016;41:9585–94. https://doi.org/10.1016/j.ijhydene.2016.02.046.

[24] Ettihir K, Higuita Cano M, Boulon L, Agbossou K. Design of an adaptive EMS for fuel cell vehicles. Int J Hydrogen Energy 2017;42(2):1481–9.

[25] Chang W-Y. Estimating equivalent circuit parameters of proton exchange membrane fuel cell using the current change method. Electrical Power Energy Syst 2013;53:584–91. https://doi.org/10.1016/j.ijepes.2013.05.031.

[26] Mann RF, Amphlett JC, Hooper MAI, Jensen HM, Peppley BA, Roberge PR. Development and application of a generalised steady-state electrochemical model for a PEM fuel cell. J Power Sources 2000;86:173–80. https://doi.org/10.1016/S0378-7753(99)00484-X.
[27] El-Fergany AA. Electrical characterisation of proton exchange membrane fuel cells stack using grasshopper optimizer. IET Renew Power Gener 2018;12:9–17. https://doi.org/10.1049/iet-rpg.2017.0232.
[28] Ali M, Elhameed MA, Farahat MA. Effective parameters' identification for polymer electrolyte membrane fuel cell models using grey wolf optimizer. Renewable Energy 2017;111:455–62. https://doi.org/10.1016/j.renene.2017.04.036.
[29] Rao Y, Shao Z, Ahangarnejad AH, Gholamalizadeh E, Sobhani B. Shark Smell Optimizer applied to identify the optimal parameters of the proton exchange membrane fuel cell model. Energy Convers Manage 2019;182:1–8. https://doi.org/10.1016/j.enconman.2018.12.057.
[30] El-Fergany AA, Hasanien HM, Agwa AM. Semi-empirical PEM fuel cells model using whale optimization algorithm. Energy Convers Manage 2019;201:112197. https://doi.org/10.1016/j.enconman.2019.112197.
[31] Sultan HM, Menesy AS, Kamel S, Tostado-Véliz M, Jurado F. Parameter Identification of Proton Exchange Membrane Fuel Cell Stacks Using Bonobo Optimizer. In: IEEE International Conference on Environment and Electrical Engineering and IEEE Industrial and Commercial Power Systems Europe (EEEIC/I&CPS Europe); 2020. p. 1–7. https://doi.org/10.1109/EEEIC/ICPSEurope49358.2020.9160597.
[32] Menesy AS, Sultan HM, Selim A, Ashmawy MG, Kamel S. Developing and applying chaotic harris hawks optimization technique for extracting parameters of several proton exchange membrane fuel cell stacks. IEEE Access 2020;8:1146–59. https://doi.org/10.1109/ACCESS.2019.2961811.
[33] Sultan HM, Menesy AS, Kamel S, Jurado F. Developing the coyote optimization algorithm for extracting parameters of proton-exchange membrane fuel cell models. Electr Eng 2021;103:563–77. https://doi.org/10.1007/s00202-020-01103-6.
[34] Selem SI, Hasanien HM, El-Fergany AA. Parameters extraction of PEMFC's model using manta rays foraging optimizer. Int J Energy Res 2020;44(6):4629–40.
[35] Singla MK, Nijhawan P, Oberoi AS. Parameter estimation of proton exchange membrane fuel cell using a novel meta-heuristic algorithm. Environ Sci Pollut Res 2021;28:34511–26. https://doi.org/10.1007/s11356-021-13097-0.
[36] Gouda EA, Kotb MF, El-Fergany AA. Jellyfish search algorithm for extracting unknown parameters of PEM fuel cell models: Steady-state performance and analysis. Energy 2021;221:119836. https://doi.org/10.1016/j.energy.2021.119836.
[37] Gouda EA, Kotb MF, El-Fergany AA. Investigating dynamic performances of fuel cells using pathfinder algorithm. Energy Convers Manage 2021;237:114099. https://doi.org/10.1016/j.enconman.2021.114099.
[38] Elsayed SK, Agwa AM, Elattar EE, El-Fergany AA. Steady-state modelling of PEM fuel cells using gradient-based optimizer. DYNA, DYNA-ACELERADO 2021;96:520–7. https://doi.org/10.6036/10099.
[39] Rizk-Allah RM, El-Fergany AA. Artificial ecosystem optimizer for parameters identification of proton exchange membrane fuel cells model. Int J Hydrogen Energy 2021;46(75):37612–27.
[40] Fawzi M, El-Fergany AA, Hasanien HM. Effective methodology based on neural network optimizer for extracting model parameters of PEM fuel cells. Int J Energy Res 2019;43:8136–47. https://doi.org/10.1002/er.4809.
[41] Gupta J, Nijhawan P, Ganguli S. Optimal parameter estimation of PEM fuel cell using slime mould algorithm. Int J Energy Res 2021;45:14732–44. https://doi.org/10.1002/er.6750.
[42] Sultan HM, Menesy AS, Kamel S, Jurado F. Tree growth algorithm for parameter identification of proton exchange membrane fuel cell models. Int J Interact Multim Artif Intell 2020;6:101–11. https://doi.org/10.9781/ijimai.2020.03.003.
[43] Zaki AA, Diab MA, Tolba AG, El-Magd A, Zaky MM, El-Rifaie AM. Fuel cell parameters estimation via marine predators and political optimizers. IEEE Access 8 2020:166998–7018. https://doi.org/10.1109/ACCESS.2020.3021754.
[44] Priya K, Rajasekar N. Application of flower pollination algorithm for enhanced proton exchange membrane fuel cell modelling. Int J Hydrogen Energy 2019;44:18438–49. https://doi.org/10.1016/j.ijhydene.2019.05.022.
[45] Wolpert DH, Macready WG. No free lunch theorems for optimization. IEEE Trans Evol Comput 1997;1:67–82. https://doi.org/10.1109/4235.585893.
[46] Guo C, Juncheng Lu, Tian Z, Guo W, Darvishan A. Optimization of critical parameters of PEM fuel cell using TLBO-DE based on Elman neural network. Energy Convers Manage 2019;183:149–58. https://doi.org/10.1016/j.enconman.2018.12.088.
[47] Sultan HM, Menesy AS, Kamel S, Selim A, Jurado F. Parameter identification of proton exchange membrane fuel cells using an improved salp swarm algorithm. Energy Convers Manage 2020;224:113341. https://doi.org/10.1016/j.enconman.2020.113341.
[48] Li J, Gao X, Cui Y, Jianjun H, Guangyin X, Zhang Z. Accurate, efficient and reliable parameter extraction of PEM fuel cells using shuffled multi-simplexes search algorithm. Energy Convers Manage 2020;206:112501. https://doi.org/10.1016/j.enconman.2020.112501.
[49] Hashim FA, Houssein EH, Hussain K, Mabrouk MS, Al-Atabany W. Honey Badger Algorithm: new metaheuristic algorithm for solving optimization problems. Math Comput Simul 2022;192:84–110. https://doi.org/10.1016/j.matcom.2021.08.013.
[50] Begg CM, Begg KS, Du Toit JT, Mills MGL. Scent-marking behaviour of the honey badger, Mellivora capensis (Mustelidae), in the southern Kalahari. Anim Behav 2003;66(5):917–29.
[51] Begg CM, Begg KS, Toit JT, Mills MGL. Life-history variables of an atypical mustelid, the honey badger Mellivora capensis. J Zool, Lond 2005;265(1):17–22.
[52] El-Fergany AA. Extracting optimal parameters of PEM fuel cells using Salp Swarm Optimizer. Renewable Energy 2018;119:641–8. https://doi.org/10.1016/j.renene.2017.12.051.
[53] Xie L, Han T, Zhou H, Zhang Z-R, Han Bo, Tang A, et al. Tuna swarm optimization: a novel swarm-based metaheuristic algorithm for global optimization. Comput Intell Neurosci 2021;2021:1–22.
[54] Naik MK, Panda R, Abraham A. An entropy minimization based multilevel colour thresholding technique for analysis of breast thermograms using equilibrium slime mould algorithm. Appl Soft Comput 2021;113:107955.
[55] Elkholy MM, El-Hay EA, El-Fergany AA. Synergy of electrostatic discharge optimizer and experimental verification for parameters estimation of three phase induction motors. Eng Sci Technol Int J 2022;31:101067.
[56] El-Hameed MA, Elkholy MM, El-Fergany AA. Three-diode model for characterization of industrial solar generating units using Manta-rays foraging optimizer: analysis and validations. Energy Convers Manage 2020;219:113048. https://doi.org/10.1016/j.enconman.2020.113048.
[57] Al R, Behera CR, Zubov A, Gernaey KV, Sin G. Meta-modeling based efficient global sensitivity analysis for wastewater treatment plants – an application to the BSM2 model. Comput Chem Eng 2019;46:127–233. https://doi.org/10.1016/j.compchemeng.2019.05.015.